

# Dark matter in galaxies: the dark matter particle mass is about 7 keV \*

H. J. de Vega <sup>(a)†</sup> and N. G. Sanchez <sup>(b)‡</sup>

<sup>(a)</sup> *LPTHE, Université Pierre et Marie Curie (Paris VI),  
Laboratoire Associé au CNRS UMR 7589, Tour 13, 4ème. et 5ème. étages,  
Boite 126, 4, Place Jussieu, 75252 Paris, Cedex 05, France.*

<sup>(b)</sup> *Observatoire de Paris, LERMA. Laboratoire Associé au CNRS UMR 8112.  
61, Avenue de l'Observatoire, 75014 Paris, France.*

(Dated: November 5, 2021)

Warm dark matter (WDM) means DM particles with mass  $m$  in the keV scale. For large scales, (structures beyond  $\sim 100$  kpc) WDM and CDM yield identical results which agree with observations. For intermediate scales, WDM gives the correct abundance of substructures. Inside galaxy cores, below  $\sim 100$  pc,  $N$ -body WDM classical physics simulations are incorrect because at such scales quantum WDM effects are important. WDM quantum calculations (Thomas-Fermi approach) provide galaxy cores, galaxy masses, velocity dispersions and density profiles in agreement with the observations. For a dark matter particle decoupling at thermal equilibrium (thermal relic), all evidences point out to a 2 keV particle. Remarkably enough, sterile neutrinos decouple out of thermal equilibrium with a primordial power spectrum similar to a 2 keV thermal relic when the sterile neutrino mass is about 7 keV. Therefore, WDM can be formed by 7 keV sterile neutrinos. Excitingly enough, Bulbul et al. (2014) announced the detection of a cluster X-ray emission line that could correspond to the decay of a 7.1 keV sterile neutrino and to a neutrino decay mixing angle of  $\sin^2 2\theta \sim 7 \cdot 10^{-11}$ . This is a further argument in favour of sterile neutrino WDM. Baryons, represent 10% of DM or less in galaxies and are expected to give a correction to pure WDM results. The detection of the DM particle depends upon the particle physics model. Sterile neutrinos with keV scale mass (the main WDM candidate) can be detected in beta decay for Tritium and Rhenium and in the electron capture in Holmium. The sterile neutrino decay into X rays can be detected observing DM dominated galaxies and through the distortion of the black-body CMB spectrum.

So far, **not a single valid** objection arose against WDM.

## Contents

<b>I. Introduction</b>	2
<b>II. Quantum Dark Matter physics in Galaxies</b>	3
A. WDM Quantum pressure vs. gravitational pressure in compact galaxies	4
<b>III. Quantum fermionic WDM gives the correct galaxy properties and cored galaxy profiles</b>	5
<b>IV. WDM gives the correct abundance of substructures</b>	12
<b>V. Detection of keV mass Sterile Neutrinos</b>	13
<b>VI. Sterile neutrinos and CMB fluctuations</b>	15
<b>VII. Detection of a 3.56 keV X-ray line in galaxy clusters</b>	15
<b>VIII. Future Perspectives and Sterile Neutrino Detection</b>	15
<b>References</b>	17

---

\* Based on Lectures given by H J de V at NuMass 2013, Milano-Bicocca, February 2013; at Cosmic Frontiers, SLAC, March 2013 and by H J de V and N G S at the Chalonge Torino Colloquium 2013, April 2013 and The Paris Chalonge Colloquium July 2014

†Electronic address: [devega@lpthe.jussieu.fr](mailto:devega@lpthe.jussieu.fr)

‡Electronic address: [Norma.Sanchez@obspm.fr](mailto:Norma.Sanchez@obspm.fr)

## I. INTRODUCTION

81 % of the matter of the universe is **dark**. Dark matter (DM) is the dominant component of galaxies. DM interacts through gravity.

DM interactions other than gravitational have been **so far unobserved**, such possible couplings must be very weak: much weaker than weak interactions in particle physics. DM is outside the standard model of particle physics.

The main proposed candidates for DM are: Neutrinos (hot dark matter) back in the 1980's with particle mass  $m \sim 1$  eV already ruled out, Cold Dark Matter (CDM), weak interacting massive particles (WIMPS) in supersymmetric models with R-parity, with particle mass  $m \sim 10 - 1000$  GeV seriously disfavoured by galaxy observations, and finally Warm Dark Matter (WDM), mainly sterile neutrinos with particle mass in the keV scale.

DM particles decouple due to the universe expansion, their distribution function **freezes out** at decoupling. The characteristic length scale after decoupling is the **free streaming scale (or Jeans' scale)**. Following the DM evolution since ultrarelativistic decoupling by solving the linear Boltzmann-Vlasov equations yields (see for example [1]),

$$r_{Jeans} = 57.2 \text{ kpc} \frac{\text{keV}}{m} \left( \frac{100}{g_d} \right)^{\frac{1}{3}}, \quad (1.1)$$

where  $g_d$  equals the number of UR degrees of freedom at decoupling.

DM particles can **freely** propagate over distances of the order of the free streaming scale. Therefore, structures at scales smaller or of the order of  $r_{Jeans}$  are **erased** for a given value of  $m$ .

The observed size of the DM galaxy substructures is in the  $\sim 1 - 100$  kpc scale. Therefore, eq.(1.1) indicates that  $m$  should be in the keV scale. That is, Warm Dark Matter particles. This indication is confirmed by the phase-space density observations in galaxies [13] and further relevant evidence from galaxy observations [3–5, 9, 15–18, 20–22].

For a dark matter particle decoupling at thermal equilibrium (thermal relic), all evidences point out to a 2 keV particle. Sterile neutrinos decouple out of thermal equilibrium with a primordial power spectrum similar to a thermal relic but for a different particle mass [2, 23]. More precisely, eq.(5.2) shows that a 7 keV sterile neutrino provides a similar primordial power than a 2 keV thermal relic.

Therefore, WDM can be formed by 7 keV sterile neutrinos. Notice that this result is independent of the sterile neutrino decay detection claimed in [51] of a 7 keV sterile neutrino decay. This is a further argument in favour of 7 keV sterile neutrino WDM (see also [53]).

For CDM particles with  $m \sim 100$  GeV we have  $r_{Jeans} \sim 0.1$  pc. Hence CDM structures keep forming till scales as small as the solar system. This result from the linear regime is confirmed as a **robust result** by  $N$ -body CDM simulations. However, it has **never been observed** in the sky.

Adding baryons to CDM does not cure this serious problem [25]. There is **over abundance** of small structures in CDM and in CDM+baryons (also called the satellite problem).

CDM has **many serious** conflicts with observations as:

- Galaxies naturally grow through merging in CDM models. Observations show that galaxy mergers are **rare** ( $< 10\%$ ).
- Pure-disk galaxies (bulgeless) are observed whose formation through CDM is unexplained.
- CDM predicts **cusped** density profiles:  $\rho(r) \sim 1/r$  for small  $r$ . Observations show **cored** profiles:  $\rho(r)$  bounded for small  $r$ . Adding by hand strong enough feedback from baryons in the CDM models can eliminate cusps but spoils the star formation rate.

Structures in the Universe as galaxies and cluster of galaxies form out of the small primordial quantum fluctuations originated by inflation just after the big-bang.

The linear small primordial fluctuations grow due to gravitational (Jeans) instabilities and then classicalize. Structures form through non-linear gravitational evolution. Hierarchical structure formation starts from small scales and develops to large scales.

$N$ -body CDM simulations **fail** to produce the observed structures for **small** scales less than some kpc.

Both  $N$ -body WDM and CDM simulations yield **identical and correct** structures for scales larger than some kpc.

At intermediate scales WDM give the **correct abundance** of substructures [18].

Inside galaxy cores, below  $\sim 100$  pc,  $N$ -body classical physics simulations are incorrect for WDM because quantum effects are important in WDM at these scales. WDM predicts correct structures for small scales (below kpc) when its **quantum** nature is taken into account [3–5].

The first ingredient in structure formation is the primordial power spectrum  $P(k)$ . We plot  $P(k)$  in fig. 1 for CDM and for several examples of WDM. CDM and WDM give identical results for the CMB fluctuations spectrum, this spectrum corresponds to large scales  $\gtrsim 1$  Mpc, in which WDM and CDM coincide.

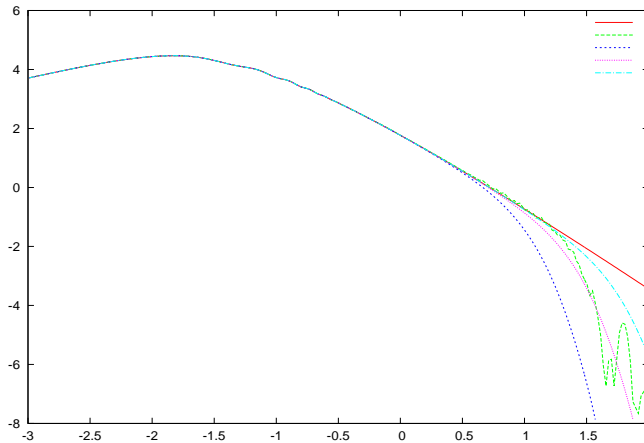


FIG. 1:  $\log_{10} P(k)$  vs.  $\log_{10}[k \text{ Mpc } h]$  for CDM in red, for 1 keV WDM in blue, 2 keV in violet and 4 keV WDM in light-blue DM particles decoupling in thermal equilibrium. 1 keV WDM sterile neutrinos decoupling out of thermal equilibrium are plotted in green. For WDM  $P(k)$  is cutted-off on small scales compared with CDM, that is  $r \lesssim 100 (\text{keV}/m)^{4/3}$  kpc.

All searches of CDM particles (wimps) look for  $m \gtrsim 1$  GeV [26]. The fact that the DM mass is in the keV scale explains why no detection has been reached so far. Moreover, past, present and future reports of signals of such CDM experiments **cannot be due to DM detection** because the DM particle mass is in the keV scale. The inconclusive signals in such experiments should be originated by phenomena of other kinds. Notice that the supposed wimp detection signals reported in refs. [26] contradict each other supporting the notion that these signals are **unrelated to any DM detection**.

Positron excess in cosmic rays are unrelated to DM physics but to astrophysical sources and astrophysical mechanisms and can be explained by them [27].

Warm dark matter has been the central subject of attention of recent Chalonge Colloquiums whose ‘Highlights and Conclusions’ are online [20].

## II. QUANTUM DARK MATTER PHYSICS IN GALAXIES

In order to determine whether a physical system has a classical or quantum nature one has to compare the average distance between particles  $d$  with their de Broglie wavelength  $\lambda_{dB}$ .

The de Broglie wavelength of DM particles in a galaxy can be expressed as

$$\lambda_{dB} = \frac{h}{m v}, \quad (2.1)$$

where  $h$  stands for Planck’s constant and  $v$  is the velocity dispersion, while the average interparticle distance  $d$  can be estimated as

$$d = \left( \frac{m}{\rho_h} \right)^{\frac{1}{3}}, \quad (2.2)$$

where  $\rho_h$  is the average density in the galaxy core. We can measure the classical or quantum character of the system by considering the ratio

$$\mathcal{R} \equiv \frac{\lambda_{dB}}{d}$$

For  $\mathcal{R} \lesssim 1$  the system is of classical nature while for  $\mathcal{R} \gtrsim 1$  it is a quantum system.

By using the phase-space density,

$$Q_h \equiv \frac{\rho_h}{\sigma^3}$$

and eqs.(2.1)-(2.2),  $\mathcal{R}$  can be expressed as [3]

$$\mathcal{R} = \hbar \frac{2\pi}{\sqrt{3}} \left( \frac{Q_h}{m^4} \right)^{\frac{1}{3}}. \quad (2.3)$$

Notice that  $\mathcal{R}$  as well as  $Q_h$  are invariant under the expansion of the universe because the lengths  $\lambda_{dB}$  and  $d$  both scale with the expansion scale factor.  $\mathcal{R}$  and  $Q_h$  evolve by nonlinear gravitational relaxation.

Using now the observed values of  $Q_h$  from Table I yields  $\mathcal{R}$  in the range

$$7 \times 10^{-3} \left( \frac{\text{keV}}{m} \right)^{\frac{4}{3}} < \mathcal{R} < 5 \left( \frac{\text{keV}}{m} \right)^{\frac{4}{3}} \quad (2.4)$$

The larger value of  $\mathcal{R}$  is for ultracompact dwarfs while the smaller value of  $\mathcal{R}$  is for big spirals.

The ratio  $\mathcal{R}$  around unity clearly implies a macroscopic quantum object. Notice that  $\mathcal{R}$  expresses solely in terms of  $Q$  and hence  $(\hbar^3 Q/m^4)$  measures how quantum or classical is the system, here, the galaxy. Therefore, eq.(2.4) clearly shows **solely from observations** that compact dwarf galaxies are natural macroscopic quantum objects for WDM [3].

We see from eq.(2.4) that for CDM, that is for  $m \gtrsim \text{GeV}$ ,

$$\mathcal{R}_{CDM} \lesssim 5 \cdot 10^{-8}$$

and therefore quantum effects are negligible in CDM.

### A. WDM Quantum pressure vs. gravitational pressure in compact galaxies

For an order-of-magnitude estimate, let us consider a halo of mass  $M$  and radius  $R$  of fermionic matter. Each fermion can be considered inside a cell of size  $\Delta x \sim 1/n^{\frac{1}{3}}$  and therefore has a momentum

$$p \sim \frac{\hbar}{\Delta x} \sim \hbar n^{\frac{1}{3}}.$$

The associated quantum pressure  $P_q$  (flux of the momentum) has the value

$$P_q = n v p \sim \hbar v n^{\frac{4}{3}} = \frac{\hbar^2}{m} n^{\frac{5}{3}}. \quad (2.5)$$

where  $v$  is the mean velocity given by

$$v = \frac{p}{m} = \frac{\hbar}{m} n^{\frac{1}{3}}.$$

The number density can be estimated as

$$n = \frac{M}{\frac{4}{3} \pi R^3 m},$$

and we obtain from eq.(2.5) the quantum pressure

$$P_q = \frac{\hbar^2}{m R^5} \left( \frac{3 M}{4 \pi m} \right)^{\frac{5}{3}}. \quad (2.6)$$

On the other hand, as is well known, galaxy formation as all structure formation in the Universe is driven by gravitational physics. The system will be in dynamical equilibrium if the quantum pressure is balanced by the gravitational pressure

$$P_G = \text{gravitational force/area} = \frac{G M^2}{R^2} \times \frac{1}{4 \pi R^2} \quad (2.7)$$

Equating  $P_q = P_G$  from eqs.(2.7)-(2.6) yields the following expressions for the size  $R$  and the velocity  $v$  in terms of the mass  $M$  of the system and the mass  $m$  of the particles [3]:

$$R = \frac{3^{\frac{5}{3}}}{(4 \pi)^{\frac{2}{3}}} \frac{\hbar^2}{G m^{\frac{8}{3}} M^{\frac{1}{3}}} = 7.8 \dots \text{pc} \left( \frac{10^4 M_\odot}{M} \right)^{\frac{1}{3}} \left( \frac{2 \text{ keV}}{m} \right)^{\frac{8}{3}}, \quad (2.8)$$

$$v = \sqrt{3} \sigma = \sqrt{3} \left( \frac{4 \pi}{81} \right)^{\frac{1}{3}} \frac{G}{\hbar} m^{\frac{4}{3}} M^{\frac{2}{3}} = 4.64 \dots \frac{\text{km}}{\text{s}} \left( \frac{m}{2 \text{ keV}} \right)^{\frac{4}{3}} \left( \frac{M}{10^4 M_\odot} \right)^{\frac{2}{3}}. \quad (2.9)$$

Notice that the values of  $M$ ,  $R$  and  $v$  are consistent with the observed values of ultracompact dwarf galaxies. Namely, for  $M$  of the order  $10^4 M_\odot$  (which is a typical mass value for an ultracompact dwarf galaxies),  $R$  and  $v$  give the correct order of magnitude for the size and velocity dispersion of dwarf galaxies as displayed in Table I, for WDM particle mass in the keV scale. These estimates are in agreement with the precise Thomas–Fermi results in the degenerate limit [5].

These results back the idea that dwarf galaxies are supported by the fermionic *WDM quantum pressure* eq.(2.6) [3].

### III. QUANTUM FERMIONIC WDM GIVES THE CORRECT GALAXY PROPERTIES AND CORED GALAXY PROFILES

We treat here the self-gravitating fermionic DM in the Thomas-Fermi approximation. In this approach, the central quantity to derive is the DM chemical potential  $\mu(r)$ , the chemical potential being the free energy per particle [28]. We consider a single DM halo in the late stages of structure formation when DM particles composing it are non-relativistic and their phase-space distribution function  $f(t, \mathbf{r}, \mathbf{p})$  is relaxing to a time-independent form, at least for  $\mathbf{r}$  not too far from the halo center. In the Thomas–Fermi approach such a time-independent form is taken to be an energy distribution function  $f(E)$  of the conserved single-particle energy  $E = p^2/(2m) - \mu$ , where  $m$  is the mass of the DM particle and  $\mu$  is the chemical potential

$$\mu(\mathbf{r}) = \mu_0 - m \phi(\mathbf{r}) \quad (3.1)$$

with  $\phi(\mathbf{r})$  the gravitational potential and  $\mu_0$  some constant. We consider the spherical symmetric case.

Here, the Poisson equation for  $\phi(r)$  is a nonlinear and selfconsistent equation

$$\frac{d^2 \mu}{dr^2} + \frac{2}{r} \frac{d\mu}{dr} = -4\pi G m \rho(r), \quad (3.2)$$

where the mass density  $\rho(r)$  is a function of  $\mu(r)$  and  $G$  is Newton's constant.  $\rho(r)$  is expressed here as a function of  $\mu(r)$  through the standard integral of the DM phase-space distribution function over the momentum for Dirac fermions as

$$\rho(r) = \frac{m}{\pi^2 \hbar^3} \int_0^\infty dp p^2 f \left( \frac{p^2}{2m} - \mu(r) \right), \quad (3.3)$$

Another standard integral of the DM phase-space distribution function is the pressure

$$P(r) = \frac{1}{3\pi^2 m \hbar^3} \int_0^\infty dp p^4 f \left( \frac{p^2}{2m} - \mu(r) \right). \quad (3.4)$$

From  $\rho(r)$  and  $P(r)$  other quantities of interest, such as the velocity dispersion  $\sigma(r)$  and the phase-space density  $Q(r)$  can be determined as

$$\sigma^2(r) = \frac{P(r)}{\rho(r)}, \quad Q(r) = \frac{\rho(r)}{\sigma^3(r)}. \quad (3.5)$$

Galaxy	$\frac{r_h}{\text{pc}}$	$\frac{v}{\frac{\text{km}}{\text{s}}}$	$\frac{\hbar^{\frac{3}{2}} \sqrt{Q_h}}{(\text{keV})^2}$	$\rho(0)/\frac{M_\odot}{(\text{pc})^3}$	$\frac{M_h}{10^6 M_\odot}$
Willman 1	19	4	0.85	6.3	0.029
Segue 1	48	4	1.3	2.5	1.93
Leo IV	400	3.3	0.2	.19	200
Canis Venatici II	245	4.6	0.2	0.49	4.8
Coma-Berenices	123	4.6	0.42	2.09	0.14
Leo II	320	6.6	0.093	0.34	36.6
Leo T	170	7.8	0.12	0.79	12.9
Hercules	387	5.1	0.078	0.1	25.1
Carina	424	6.4	0.075	0.15	32.2
Ursa Major I	504	7.6	0.066	0.25	33.2
Draco	305	10.1	0.06	0.5	26.5
Leo I	518	9	0.048	0.22	96
Sculptor	480	9	0.05	0.25	78.8
Boötes I	362	9	0.058	0.38	43.2
Canis Venatici I	1220	7.6	0.037	0.08	344
Sextans	1290	7.1	0.021	0.02	116
Ursa Minor	750	11.5	0.028	0.16	193
Fornax	1730	10.7	0.016	0.053	1750
NGC 185	450	31	0.033	4.09	975
NGC 855	1063	58	0.01	2.64	8340
Small Spiral	5100	40.7	0.0018	0.029	6900
NGC 4478	1890	147	0.003	3.7	$6.55 \times 10^4$
Medium Spiral	$1.9 \times 10^4$	76.2	$3.7 \times 10^{-4}$	0.0076	$1.01 \times 10^5$
NGC 731	6160	163	$9.27 \times 10^{-4}$	0.47	$2.87 \times 10^5$
NGC 3853	5220	198	$8.8 \times 10^{-4}$	0.77	$2.87 \times 10^5$
NGC 499	7700	274	$5.9 \times 10^{-4}$	0.91	$1.09 \times 10^6$
Large Spiral	$5.9 \times 10^4$	125	$0.96 \times 10^{-4}$	$2.3 \times 10^{-3}$	$1. \times 10^6$

TABLE I: Observed values  $r_h$ , velocity dispersion  $v$ ,  $\sqrt{Q_h}$ ,  $\rho(0)$  and  $M_h$  covering from ultracompact galaxies to large spiral galaxies from refs.[6–11]. The phase space density is larger for smaller galaxies, both in mass and size. Notice that the phase space density is obtained from the stars velocity dispersion which is expected to be smaller than the DM velocity dispersion. Therefore, the reported  $Q_h$  are in fact upper bounds to the true values [10].

We see that  $\mu(r)$  fully characterizes the fermionic DM halo in this Thomas–Fermi framework. The chemical potential is monotonically decreasing in  $r$  since eq. (3.2) implies

$$\frac{d\mu}{dr} = -\frac{G m M(r)}{r^2} \quad , \quad M(r) = 4\pi \int_0^r dr' r'^2 \rho(r') \quad . \quad (3.6)$$

Moreover, the fermionic DM mass density  $\rho$  is bounded at the origin due to the Pauli principle [3], and therefore the proper boundary condition at the origin is

$$\frac{d\mu}{dr}(0) = 0 \quad . \quad (3.7)$$

Eqs.(3.2) and (3.3) provide an ordinary nonlinear differential equation that determines selfconsistently the chemical potential  $\mu(r)$  and constitutes the Thomas–Fermi semi-classical approach [3–5] (see also ref. [24]). We obtain a family of solutions parametrized by the value of  $\mu_0 \equiv \mu(0)$  [3].

In this semi-classical framework the stationary energy distribution function  $f(E)$  must be assigned beforehand. In a full–fledged treatment one would solve the cosmological WDM evolution since decoupling till today, including the

quantum WDM dynamics in the evolution which become important in the non-linear stage and close enough to the origin.

We integrate the Thomas-Fermi nonlinear differential equations (3.2)-(3.3) from  $r = 0$  till the boundary  $r = R = R_{200} \sim R_{vir}$  defined as the radius where the mass density equals 200 times the mean DM density [3].

We define the core size  $r_h$  of the halo by analogy with the Burkert density profile as

$$\frac{\rho(r_h)}{\rho_0} = \frac{1}{4} \quad , \quad r_h = l_0 \xi_h . \quad (3.8)$$

where  $\rho_0 \equiv \rho(0)$  and  $l_0$  is the characteristic length that emerges from the dynamical equations (3.2)-(3.3):

$$l_0 \equiv \frac{\hbar}{\sqrt{8G}} \left( \frac{9\pi}{m^8 \rho_0} \right)^{\frac{1}{6}} = R_0 \left( \frac{\text{keV}}{m} \right)^{\frac{4}{3}} \left( \rho_0 \frac{\text{pc}^3}{M_\odot} \right)^{-\frac{1}{6}} , \quad R_0 = 18.71 \text{ pc} . \quad (3.9)$$

To explicitly solve eqs.(3.2)-(3.3) we need to specify the distribution function  $\Psi(E/E_0)$ . But many important properties of the Thomas-Fermi semi-classical approximation do not depend on the detailed form of the distribution function  $\Psi(E/E_0)$ . Indeed, a generic feature of a physically sensible one-parameter form  $\Psi(E/E_0)$  is that it should describe degenerate fermions for  $E_0 \rightarrow 0$ . That is,  $\Psi(E/E_0)$  should behave as the step function  $\theta(-E)$  in such limit. In the opposite limit,  $\mu/E_0 \rightarrow -\infty$ ,  $\Psi(E/E_0)$  describes classical particles, namely a Boltzmann distribution. As an example of distribution function, we consider the Fermi-Dirac distribution

$$\Psi_{\text{FD}}(E/E_0) = \frac{1}{e^{E/E_0} + 1} . \quad (3.10)$$

We define the dimensionless chemical potential  $\nu(r)$  as

$$\nu(r) \equiv \mu(r)/E_0 \quad \text{and} \quad \nu_0 \equiv \mu(0)/E_0 .$$

Positive values of the chemical potential at the origin  $\nu_0 > 1$  correspond to the fermions in the quantum regime, and oppositely,  $\nu_0 < -1$  gives the diluted regime which is the classical regime. In this classical regime the Thomas-Fermi equations (3.2)-(3.3) become exactly the equations for a self-gravitating Boltzmann gas.

Normalizing the density profiles as  $\rho(r)/\rho(0)$  and plotting them as functions of  $r/r_h$  produce normalized profiles which are **universal** functions of  $x \equiv r/r_h$  in the diluted regime as shown in fig. 2. This universality is valid for **all** galaxy masses  $\hat{M}_h > 10^5 M_\odot$  [5]. The obtained fermion profiles are always cored.

Our theoretical density profiles and rotation curves obtained from the Thomas-Fermi equations remarkably agree with observations for  $r \lesssim r_h$ , for all galaxies in the diluted regime [4]. This indicates that WDM is thermalized in the internal regions  $r \lesssim r_h$  of galaxies [5].

For galaxy masses  $\hat{M}_h < 10^5 M_\odot$ , near the quantum degenerate regime, the normalized density profiles  $\rho(r)/\rho(0)$  are not anymore universal and depend on the galaxy mass.

As we can see in fig. 2 the density profile shape changes fastly when the galaxy mass decreases only by a factor seven from  $\hat{M}_h = 1.4 \cdot 10^5 M_\odot$  to the minimal galaxy mass  $\hat{M}_{h,min} = 3.10 \cdot 10^4 M_\odot$ . In this narrow range of galaxy masses the density profiles shrink from the universal profile till the degenerate profile as shown in fig. 2. Namely, these dwarf galaxies are more compact than the larger diluted galaxies.

We display in fig. 3 the normalized velocity dispersion profiles  $\sigma^2(r)/\sigma^2(0)$  as functions of  $x = r/r_h$ . Again, we see that these profiles are **universal and constant**, i. e. independent of the galaxy mass in the diluted regime for  $M_h > 2.3 \cdot 10^6 M_\odot$ ,  $\nu_0 < -5$ ,  $T_0 > 0.017$  K. The constancy of  $\sigma^2(r) = \sigma^2(0)$  in the diluted regime implies that the equation of state is that of a perfect but inhomogeneous WDM gas [5]

$$P(r) = \frac{1}{3} \langle v^2 \rangle (r) \rho(r) = \sigma^2(r) \rho(r) \quad , \quad \sigma^2(r) = \sigma^2(0) = \frac{T_0}{m} , \quad (3.11)$$

WDM diluted galaxies exhibit a perfect gas equation of state where both the pressure  $P(r)$  and the density  $\rho(r)$  depend on the coordinates.

For smaller galaxy masses  $1.6 \cdot 10^6 M_\odot > \hat{M}_h > \hat{M}_{h,min}$ , the velocity profiles do depend on  $r$  and yield decreasing velocity dispersions for decreasing galaxy masses. Namely, the deviation from the universal curves appears for  $\hat{M}_h < 10^6 M_\odot$  and we see that it precisely arises from the quantum fermionic effects which become important in such range of galaxy masses.

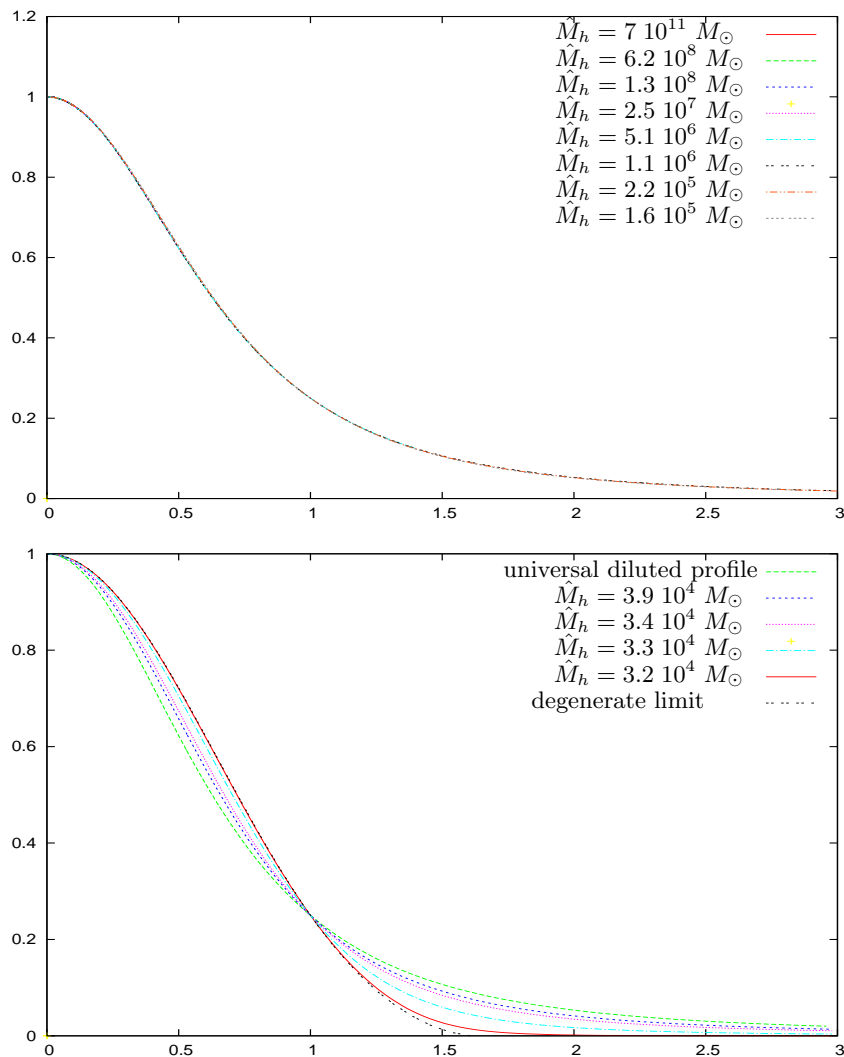


FIG. 2: Normalized density profiles  $\rho(r)/\rho(0)$  as functions of  $r/r_h$ . We display in the upper panel the profiles for galaxy masses in the diluted regime  $1.4 \cdot 10^5 M_\odot < \hat{M}_h < 7.5 \cdot 10^{11} M_\odot$ ,  $-1.5 > \nu_0 > -20.78$  which **all** provide the **same universal** density profile. We display in the lower panel the profiles for galaxy masses  $M_h^{min} = 30999 (2 \text{ keV}/m)^{\frac{16}{5}} M_\odot \leq \hat{M}_h < 3.9 \cdot 10^4 M_\odot$ ,  $1 < \nu_0 < \infty$  which are near the quantum degenerate regime and exhibit shrinking density profiles for decreasing galaxy mass. For comparison, we also plot in the lower figure the universal profile in the diluted regime.

The sizes of the cores  $r_h$  defined by eq.(3.8) are in agreement with the observations, from the compact galaxies where  $r_h \sim 35$  pc till the spiral and elliptical galaxies where  $r_h \sim 0.2 - 60$  kpc. The larger and positive is  $\nu_0$ , the smaller is the core. The minimal core size arises in the degenerate case  $\nu_0 \rightarrow +\infty$  (compact dwarf galaxies).

We plot in fig. 6 the ordinary logarithm of the theoretical Thomas-Fermi phase-space density  $\log_{10} Q_{TF}/\text{keV}^4$  vs. the ordinary logarithm of  $\hat{M}_h$  and the observational values of  $\log_{10} Q_{Bur}/\text{keV}^4$ . We see that the theoretical phase-space density  $Q_{TF}$  reproduces very well the observational data [4].

We **derive** the general equation of state for galaxies, i. e., the relation between pressure and density, and provide its analytic expression [5]. Two regimes clearly show up: (i) Large diluted galaxies for  $M_h \gtrsim 2.3 \cdot 10^6 M_\odot$  and effective temperatures  $T_0 > 0.017$  K described by the classical selfgravitating WDM Boltzman gas with an inhomogeneous perfect gas equation of state, and (ii) Compact dwarf galaxies for  $1.6 \cdot 10^6 M_\odot \gtrsim M_h \gtrsim M_{h,min} \simeq 3.10 \cdot 10^4 (2 \text{ keV}/m)^{\frac{16}{5}} M_\odot$ ,  $T_0 < 0.011$  K described by the quantum fermionic WDM regime with a steeper equation of state close to the degenerate state. In particular, the  $T_0 = 0$  degenerate or extreme quantum limit yields the most compact and smallest galaxy. All magnitudes in the diluted regime turn to exhibit square root of  $M_h$  **scaling** laws and are **universal** functions of  $r/r_h$  reflecting the WDM perfect gas behaviour in this regime. These theoretical results contrasted to robust and independent sets of galaxy data remarkably reproduce the observations. For the



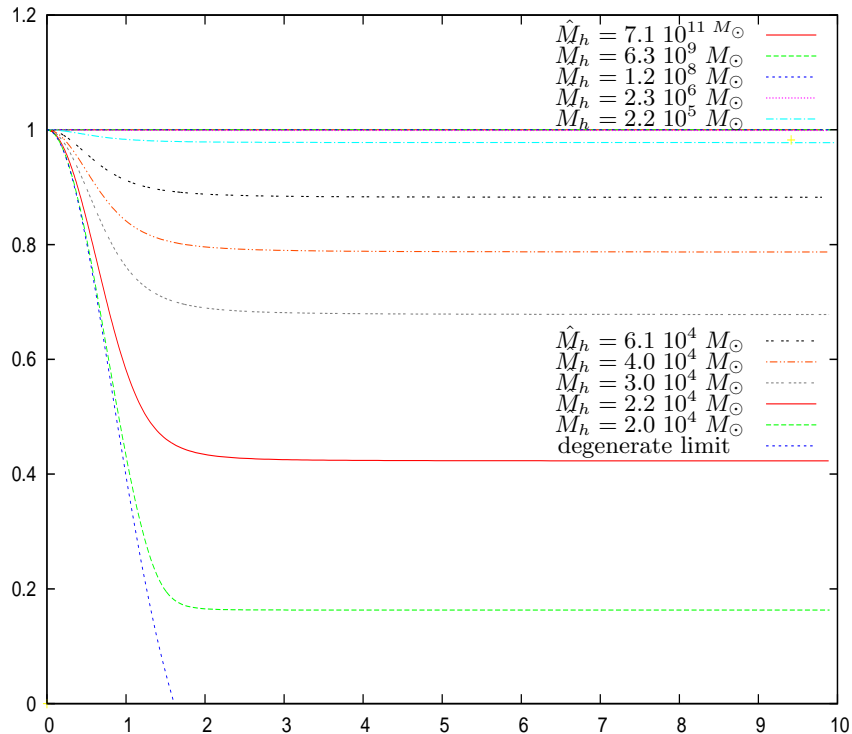


FIG. 3: Normalized velocity dispersion profiles  $\sigma^2(r)/\sigma^2(0)$  as functions of  $x = r/r_h$ . All velocity profiles in the diluted regime for galaxy masses  $\hat{M}_h > 2.3 \cdot 10^6 M_\odot$ ,  $\nu_0 < -5$  fall into the same **constant universal** profile corresponding to a perfect but inhomogeneous self-gravitating WDM gas describing large and diluted galaxies. The velocity profiles for smaller galaxy masses  $1.6 \cdot 10^6 M_\odot > \hat{M}_h > \hat{M}_{h,min} = 3.10 \cdot 10^4 M_\odot$  do depend on  $x$  and yield decreasing velocity dispersions for decreasing galaxy masses, accounting for the quantum fermionic effects which become important in this range of galaxy masses (WDM compact dwarf galaxies).

small galaxies,  $10^6 \gtrsim M_h \geq M_{h,min}$ , the equation of state is galaxy mass dependent and the density and velocity profiles are not anymore universal, accounting to the quantum physics of the self-gravitating WDM fermions in the compact regime (near, but not at, the degenerate state). It would be extremely interesting to dispose of dwarf galaxy observations which could check these quantum effects.

We find that all magnitudes in the diluted regime exhibit square root of  $M_h$  **scaling** laws and are **universal** functions of  $r/r_h$  normalized to their values at the origin or at  $r_h$ . Conversely, the halo mass  $M_h$  scales as the square of the halo radius  $r_h$  as

$$M_h = 1.75572 \Sigma_0 r_h^2 \quad .$$

Moreover, the proportionality factor in this scaling relation is confirmed by the galaxy data (see fig. 2).

The phase space density decreases from its maximum value for the compact dwarf galaxies corresponding to the limit of degenerate fermions till its smallest value for large galaxies, spirals and ellipticals, corresponding to the classical dilute regime. On the contrary, the halo radius  $r_h$  and the halo mass  $M_h$  monotonically increase from the quantum (small and compact galaxies) to the classical regime (large and dilute galaxies).

Thus, the whole range of values of the chemical potential at the origin  $\nu_0$  from the extreme quantum (degenerate) limit  $\nu_0 \gg 1$  to the classical (Boltzmann) dilute regime  $\nu_0 \ll -1$  yield all masses, sizes, phase space densities and velocities of galaxies from the ultra compact dwarfs till the larger spirals and elliptical in agreement with the observations (see Table I).

In addition, the galaxy velocity dispersions turn to be fully consistent with the galaxy observations in Table I [3].

Adding baryons to CDM simulations have been often invoked to solve the serious CDM problems at small scales. It must be noticed however that the excess of substructures in CDM happens in DM dominated halos where baryons are especially subdominant and hence the effects of baryons cannot drastically modify the overabundance of substructures of the pure CDM results.

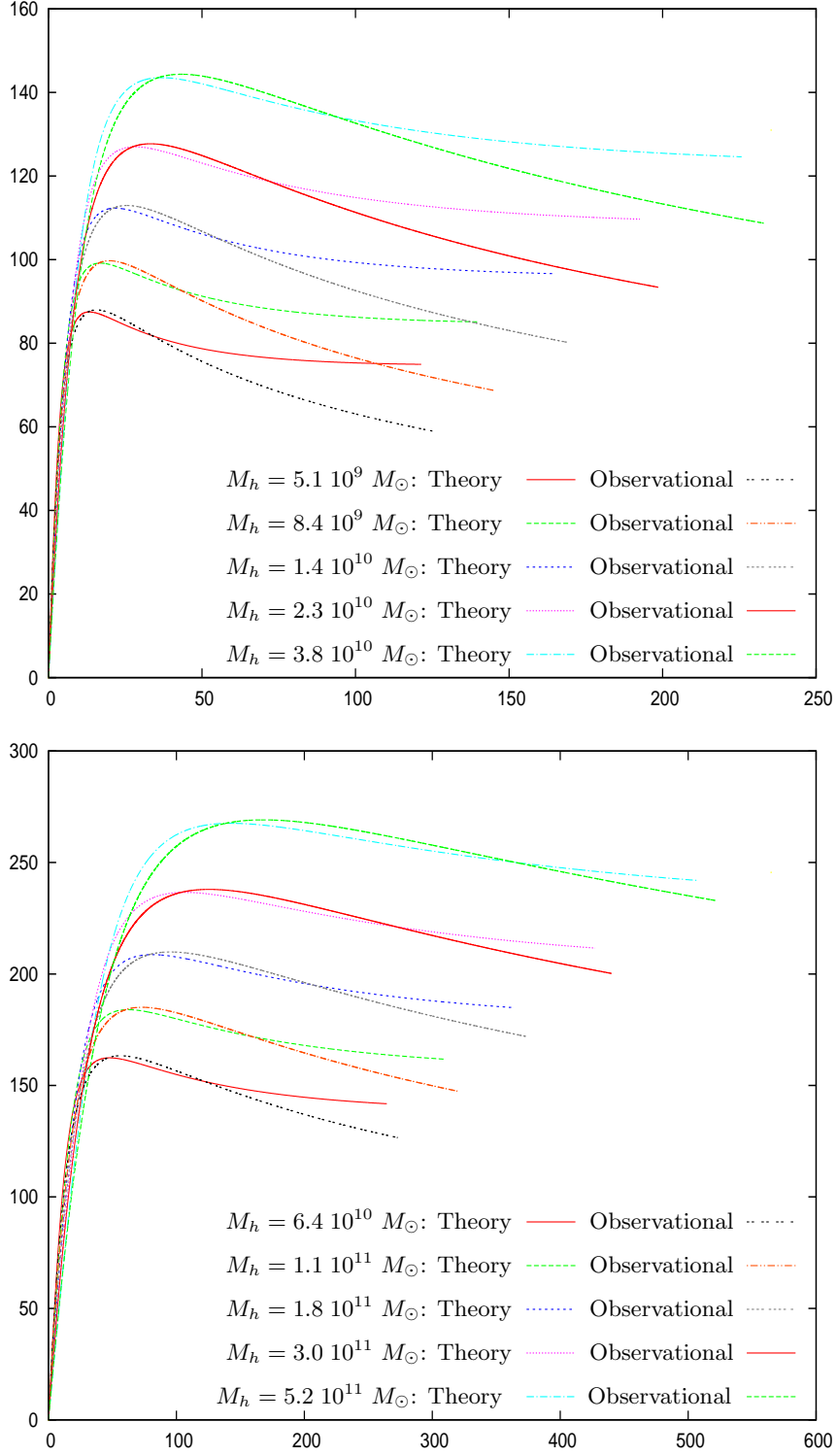


FIG. 4: The velocity rotation curves  $v_c(r)$  in km/s versus  $r$  in kpc for ten different independent galaxy masses  $M_h$  going from  $5.13 \cdot 10^9 M_\odot$  till  $5.15 \cdot 10^{11} M_\odot$ . For each galaxy mass  $M_h$ , we show the two curves: the theoretical Thomas-Fermi curve and the observational Burkert curve. The Thomas-Fermi curves reproduce remarkably well the observational curves for  $r \lesssim r_h$  [4]. We plot  $v_c(r)$  for  $0 < r < r_{vir}$ ,  $r_{vir}$  being the virial radius of the galaxy.

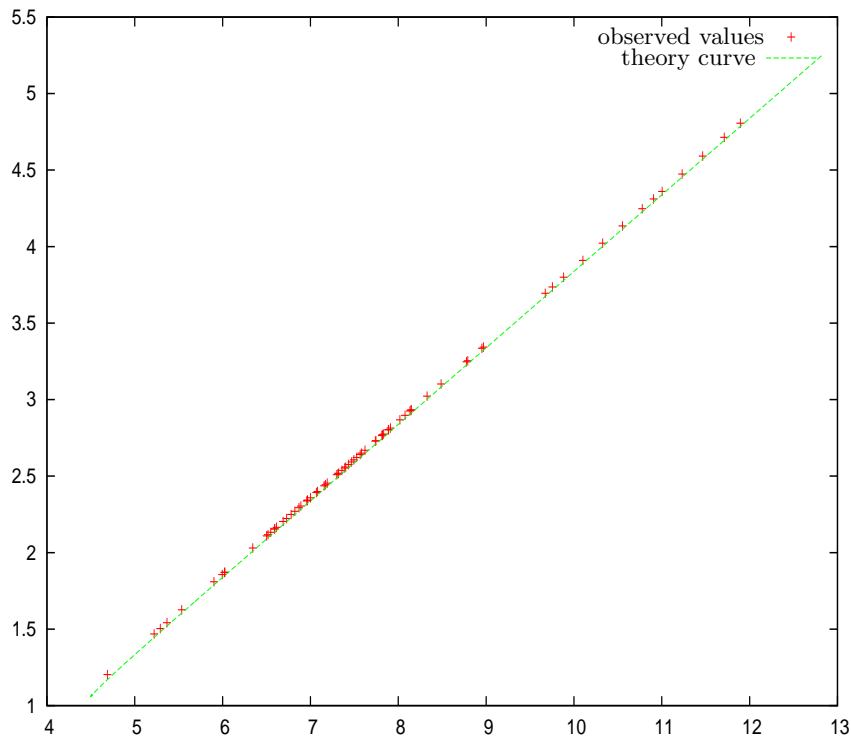


FIG. 5: The ordinary logarithm of  $\hat{r}_h = \frac{r_h}{\text{pc}} \left( \frac{\Sigma_0 \text{ pc}^2}{120 M_\odot} \right)^{\frac{1}{5}}$  vs. the ordinary logarithm of  $\hat{M}_h = \frac{M_h}{M_\odot} \left( \frac{120 M_\odot}{\Sigma_0 \text{ pc}^2} \right)^{\frac{3}{5}}$ . We see that  $r_h$  follows with precision the square-root of  $M_h$  as in the dilute regime of the Thomas-Fermi equations [5]. The data for  $M_h$  and  $r_h$  are taken from Table 1 in [3], from [12] and from [8] and they are satisfactorily reproduced by the theoretical Thomas-Fermi curve.

The influence of baryon feedback into CDM cusps of density profiles depends on the strength of the feedback. For normal values of the feedback, baryons produce adiabatic contraction and the cusps in the density profiles become even more cuspy.

Using the baryon feedback as a free parameter, it is possible to exaggerate the feedback such to destroy the CDM cusps but then, the star formation ratio disagrees with the available and precise astronomical observations. Moreover, "semi-analytic (CDM + baryon) models" have been introduced which are just empirical fits and prescriptions to some galaxy observations.

In addition, there are serious evolution problems in CDM galaxies: for instance pure-disk galaxies (bulgeless) are observed whose formation through CDM is unexplained.

In summary, adding baryons to CDM simulations bring even more serious discrepancies with the set of astronomical observations.

We consider spherical symmetry in our approach for simplicity to determine the essential physical galaxy properties as the classical or quantum nature of galaxies, compact or dilute galaxies, the phase space density values, the cored nature of the mass density profiles, the galaxy masses and sizes [3–5]. It is clear that DM halos are not perfectly spherical but describing them as spherically symmetric is a first approximation to which other effects can be added. In ref. [3] we estimated the angular momentum effect and this yields small corrections. The quantum or classical galaxy nature, the cusped or cored nature of the density profiles in the central halo regions can be captured in the spherically symmetric treatment.

Our spherically symmetric treatment captures the essential features of the gravitational dynamics and agree with the observations. Notice that we are treating the DM particles quantum mechanically through the Thomas-Fermi approach, so that expectation values are independent of the angles (spherical symmetry) but the particles move and fluctuate in all directions. Namely, this is more than treating purely classical orbits for particles in which only radial motion is present. The Thomas-Fermi approach can be generalized to describe non-spherically symmetric and non-isotropic situations, by considering distribution functions which include other particle parameters like the angular momentum.

To conclude, the galaxy magnitudes: halo radius, galaxy masses and velocity dispersion obtained from the Thomas-

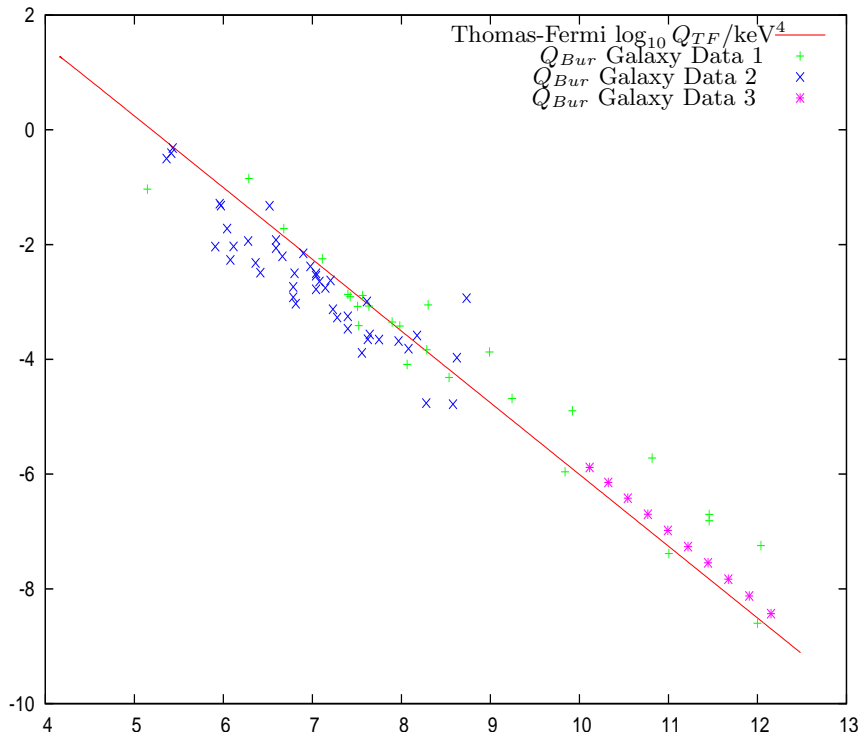


FIG. 6: The theoretical Thomas-Fermi  $\log_{10} Q_{TF}/\text{keV}^4$  phase-space density vs. the halo mass  $\log_{10} \hat{M}_h$ . The theoretical curve  $Q_{TF}$  is obtained from the Thomas-Fermi expression [4]. The data for  $Q_{Bur}$  have been obtained from circular velocities. Galaxy Data 1 refers to data from Table 1 in [3], Galaxy Data 2 refers to data from [12] and Galaxy Data 3 refers to data from [8].

Fermi quantum treatment for WDM fermion masses in the keV scale are fully consistent with all the observations for all types of galaxies (see Table I). Namely, fermionic WDM treated quantum mechanically, as it must be, is able to reproduce the observed DM cores and their sizes in galaxies [3–5]. These results strenght the discussion in sec. II A that compact galaxies are supported against gravity by the fermionic WDM quantum pressure.

It is highly remarkably that in the context of fermionic WDM, the simple stationary quantum description provided by the Thomas-Fermi approach is able to reproduce such broad variety of galaxies.

Baryons have not yet included in the present study. This is fully justified for dwarf compact galaxies which are composed today 99.99% of DM. In large galaxies the baryon fraction can reach values up to 1 - 3 %. Fermionic WDM by itself produces galaxies and structures in agreement with observations for all types of galaxies, masses and sizes. Therefore, the effect of including baryons is expected to be a correction to these pure WDM results, consistent with the fact that dark matter is in average six times more abundant than baryons.

#### IV. WDM GIVES THE CORRECT ABUNDANCE OF SUBSTRUCTURES

It is known since some time through  $N$ -body simulations that WDM alleviates the CDM satellite problem [15, 16] and the CDM voids problem [17].

WDM subhalos turns to be less concentrated than CDM subhalos. WDM subhalos have the right concentration to host the bright Milky Way satellites [16].

The ALFALFA survey has measured the velocity widths in galaxies from the 21cm HI line. This is a test for substructure formation. The confrontation of the ALFALFA survey with the substructures from  $N$ -body simulations clearly favours WDM over CDM [18]. A particle mass around  $\sim 2$  keV is favoured by the ALFALFA survey.

In summary, WDM produces the correct substructure abundance at zero redshift.

Data on galaxy substructure for redshift  $z \lesssim 10$  becomes now available.

In ref. [21] the evolution of the observed AGN luminosity function for  $3 < z < 6$  is contrasted with the WDM and CDM simulations. WDM is clearly favoured over CDM by the observational data.

In ref. [23] the number of observed structures vs. the theoretical Press-Schechter estimation for  $z = 5, 6, 7$  and  $8$  is contrasted with the results from WDM and CDM simulations. Again, WDM turns to be clearly favoured by the observations over CDM.

At intermediate scales where WDM and CDM give non-identical results and quantum effects are negligible,  $N$ -body classical simulations are reliable. Contrasting such  $N$ -body classical simulations results with astronomical observations at zero and non-zero redshifts **clearly favours** WDM over CDM.

For larger scales  $\gtrsim 100$  kpc, CDM and WDM  $N$ -body classical simulations are reliable and give identical results in good agreement with astronomical and cosmological observations.

## V. DETECTION OF KEV MASS STERILE NEUTRINOS

Sterile neutrinos  $\nu_s$  are mainly formed by right-handed neutrinos  $\nu_R$  plus a small amount of left-handed neutrinos  $\nu_L$ . Conversely, active neutrinos  $\nu_e$  are formed by  $\nu_L$  plus a small amount of  $\nu_R$ :

$$\nu_s \simeq \nu_R + \theta \nu_L \quad , \quad \nu_a = \nu_L + \theta \nu_R .$$

The name sterile neutrino was introduced by Bruno Pontecorvo in 1968. They are singlets under all symmetries of the Standard Model of particle physics. Sterile neutrinos do not interact through weak, electro-magnetic or strong interactions.

WDM  $\nu_s$  are typically produced in the early universe from active neutrinos through mixing, namely, through a bilinear term  $\theta \nu_s \nu_a$  in the Lagrangian.

The appropriate value of the mixing angle  $\theta$  to produce enough sterile neutrinos  $\nu_s$  accounting for the observed total DM depends on the particle physics model and is typically very small:

$$\theta \sim 10^{-3} - 10^{-4} .$$

The smallness of  $\theta$  makes sterile neutrinos difficult to detect in experiments.

Sterile neutrinos can be detected in beta decay and in electron capture (EC) processes when a  $\nu_s$  with mass in the keV scale is produced **instead** of an active  $\nu_a$ :

$${}^3H_1 \implies {}^3He_2 + e^- + \bar{\nu}_e \quad , \quad {}^{187}Re \implies {}^{187}Os + e^- + \bar{\nu}_e .$$

In beta decays when a  $\bar{\nu}_s$  is produced instead of a  $\bar{\nu}_e$  in the decay products the electron spectrum is slightly modified at energies around the  $\nu_s$  mass ( $\sim$  keV). Such event can be inferred observing the electron energy spectrum. A 'kink' should then appear around the energy of the  $\nu_s$  mass.

In electron capture processes like:

$${}^{163}Ho + e^- \implies {}^{163}Dy^* + \nu_e ,$$

when a sterile neutrino  $\nu_s$  with mass in the keV scale is produced **instead** of an active  $\nu_e$ , the observed nonradiative de-excitation of the excited Dysprosium  $Dy^*$  is different to the case where an active  $\nu_e$  shows up.

The available energies for these beta decays and EC are

$$Q({}^{187}Re) = 2.47 \text{ keV} \quad , \quad Q({}^3H_1) = 18.6 \text{ keV} \quad , \quad Q({}^{163}Ho) \simeq 2.5 \text{ keV}. \quad (5.1)$$

In order to produce a sterile neutrino with mass  $m$ ,  $Q$  must be larger than  $m$ . However, in order to distinguish the sterile neutrino  $\nu_s$  from a practically massless active neutrino  $\nu_a$ ,  $Q$  must be as small as possible. This motivates the choice of the nuclei with the lowest known  $Q$  in eq.(5.1).

For a theoretical analysis of  $\nu_s$  detection in Rhenium and Tritium beta decay see ref.[29] and references therein.

Present experiments searching the small active neutrino mass also look for sterile neutrinos in the keV scale:

- MARE (Milan, Italy), Rhenium 187 beta decay and Holmium 163 electron capture [34].

- KATRIN (Karlsruhe, Germany), Tritium beta decay [35, 36].
- ECHo (Heidelberg, Germany), Holmium 163 EC [37].
- Project 8 (Seattle, USA), Tritium beta decay [38].
- PTOLEMY experiment: Princeton Tritium Observatory. Aims to detect the cosmic neutrino background and WDM (keV scale) sterile neutrinos through the electron spectrum of the Tritium beta decay induced by the capture of a cosmic neutrino or a WDM sterile neutrino [41].
- HOLMES electron capture in  $^{163}\text{Ho}$  calorimeter Gran Sasso

The more popular sterile neutrino models nowadays are:

- The Dodelson-Widrow (DW) model (1994): sterile neutrinos are produced by non-resonant mixing from active neutrinos.
- The Shi-Fuller model (SF) (1998): sterile neutrinos are produced by resonant mixing from active neutrinos.
- $\nu\text{MSM}$  model (2005): sterile neutrinos are produced by a Yukawa coupling from the decay of a heavy real scalar field  $\chi$ .
- And in addition, there exists a variety of sterile neutrino models based on the Froggatt-Nielsen mechanism, flavor symmetries,  $Q_6$ , split see-saw, extended see-saw, inverse see-saw, loop mass. Furthermore: scotogenic, LR symmetric models, etc. See for a recent review [30].

The primordial power spectra of WDM particles decoupling ultrarelativistically and out of equilibrium in the first three WDM sterile neutrino models above (DW, SF and  $\nu\text{MSM}$ ) behave in a similar way just as if their masses were different [2]. The masses of the WDM sterile neutrinos in the first three models which give the same primordial power spectrum are related according to the formula [2] (FD = thermal fermions):

$$\frac{m_{DW}}{\text{keV}} \simeq 2.85 \left( \frac{m_{FD}}{\text{keV}} \right)^{\frac{4}{3}}, \quad m_{SF} \simeq 2.55 m_{FD}, \quad m_{\nu\text{MSM}} \simeq 1.9 m_{FD}. \quad (5.2)$$

(Here SF corresponds to the SF model without lepton asymmetry).

The primordial spectra of DW, SF and  $\nu\text{MSM}$  models are equal between themselves and equal to the thermal relic power spectrum when the relations eq.(5.2) hold.

On the other hand, sterile neutrinos  $\nu_s$  decay into active neutrinos  $\nu_a$  plus X-rays with an energy  $m/2$  [31]. The lifetime of  $\nu_s$  is about  $\sim 10^{11} \times$  age of the universe. The value of the lifetime depends on the particle physics neutrino model.

These X-rays may be seen in the sky looking to galaxies [32]. See [33] for a recent review.

Some future observations of X-rays from galaxy halos are:

- DM bridge between M81 and M82  $\sim 50$  kpc. Overlap of DM halos. Satellite projects: Xenia (NASA) [39]. ASTRO-H (Japan) [40].

Some WDM hints from the CMB are:

- WDM decay distorts the blackbody CMB spectrum. The projected PIXIE satellite mission can measure the WDM sterile neutrino mass by measuring this distortion [42].

Active neutrinos are very abundant in supernovae explosions and in these explosions sterile neutrinos are produced too. Hence, bounds on the presence of sterile neutrinos can be obtained contrasting to supernovae observations. The results from supernovae do not constrain  $\theta$  provided  $1 < m < 10$  keV [43].

## VI. STERILE NEUTRINOS AND CMB FLUCTUATIONS

CMB fluctuations data provide the effective number of neutrinos,  $N_{\text{eff}}$ . This effective number  $N_{\text{eff}}$  is related in a subtle way to the real number (three) of active neutrinos plus the number of sterile neutrinos with masses much smaller than the electron mass  $m_e$  [44].

WDM should decouple early at temperatures beyond the Fermi scale because DM is not in the Standard Model of Particle Physics (SM). WDM couples to the SM particles much weakly than weak interactions. Therefore, the number of ultrarelativistic degrees of freedom at decoupling  $g(T_d)$  includes all SM particles and probably beyond. We have  $g_{SM} = 427/4$  for the SM and  $g_{MSSM} = 915/4$  for the minimal supersymmetric SM.

Entropy conservation determines the WDM contribution to the effective number of neutrinos  $N_{\text{eff}}$  [45]. One keV scale WDM sterile neutrino decoupling at the temperature  $T_d$  contributes to  $N_{\text{eff}}$  at recombination by

$$\Delta N^{WDM} = \left( \frac{T_d}{T_{rc}} \right)^4 = \left[ \frac{g_{rc}}{g(T_d)} \right]^{4/3}, \quad \text{rc stands for recombination.} \quad (6.1)$$

At recombination  $z = 1090$ , we have  $g_{rc} = 29/4$  and eq.(6.1) gives for the SM and the MSSM:

$$\Delta N_{SM}^{WDM} = 0.02771 \dots, \quad \Delta N_{MSSM}^{WDM} = 0.01003 \dots$$

Such keV WDM contributions to the effective number of neutrinos  $N_{\text{eff}}$  are too small to be measurable by the present CMB anisotropy observations. Hence, Planck and WMAP results cannot provide information about these keV sterile neutrino WDM contributions.

However, Planck results [46] are **compatible** with one or two Majorana sterile neutrinos in the eV mass scale [44]. The possibility of a eV sterile neutrino is important for the whole subject of neutrinos and hence for WDM. The existence of one sterile neutrino in the eV scale opens the possibility of sterile neutrinos suggesting the existence of further sterile neutrinos with different masses, including a keV mass WDM sterile neutrino.

## VII. DETECTION OF A 3.56 KEV X-RAY LINE IN GALAXY CLUSTERS

E.Bulbul et al. [51] reported the detection of a new X-ray line in galaxy clusters that may be originated by the decay of a 7.1 keV sterile neutrino. Sterile neutrinos remain out of thermal equilibrium today.

The line flux detected in the full sample corresponds to a mixing angle for the decay [51]

$$\sin^2 2\theta \sim 7 \times 10^{-11}$$

This mixing angle value is below the upper limits placed by the previous searches.

From the conversion formulas eq.(5.2), a 7.1 keV DW sterile neutrino behaves as a 1.99 keV thermal relic, and a 7.1 keV SF sterile neutrino behaves as a 2.8 keV thermal relic. In addition, a 7.1 keV SF sterile neutrino with lepton asymmetry yields similar results [53].

WDM thermal relics with thermal mass near 2 keV provide the correct small scale structure formation and galaxy structures. Therefore, the main known sterile neutrino particle models provide a 7.1 keV sterile neutrino and the same structure formation results of a 2 keV thermal relic.

Therefore, a 7.1 keV sterile neutrino may be plausibly the dark matter particle !

Confirmation of the detection and identification of the 3.56 keV X-ray line from Astro-H is awaited for 2015 !

If a relic decoupling at thermal equilibrium would be the WDM, then the favoured physical mass would be about 2 keV. This would require WDM particle models different from sterile neutrinos.

## VIII. FUTURE PERSPECTIVES AND STERILE NEUTRINO DETECTION

WDM particle models must explain the baryon asymmetry of the universe. This is a strong constraint on sterile neutrino models which must be worked out for each model.

Combining particle, cosmological and galaxy results for sterile neutrinos at different mass scales [3, 13, 47–49], an appealing **mass** neutrino hierarchy appears:

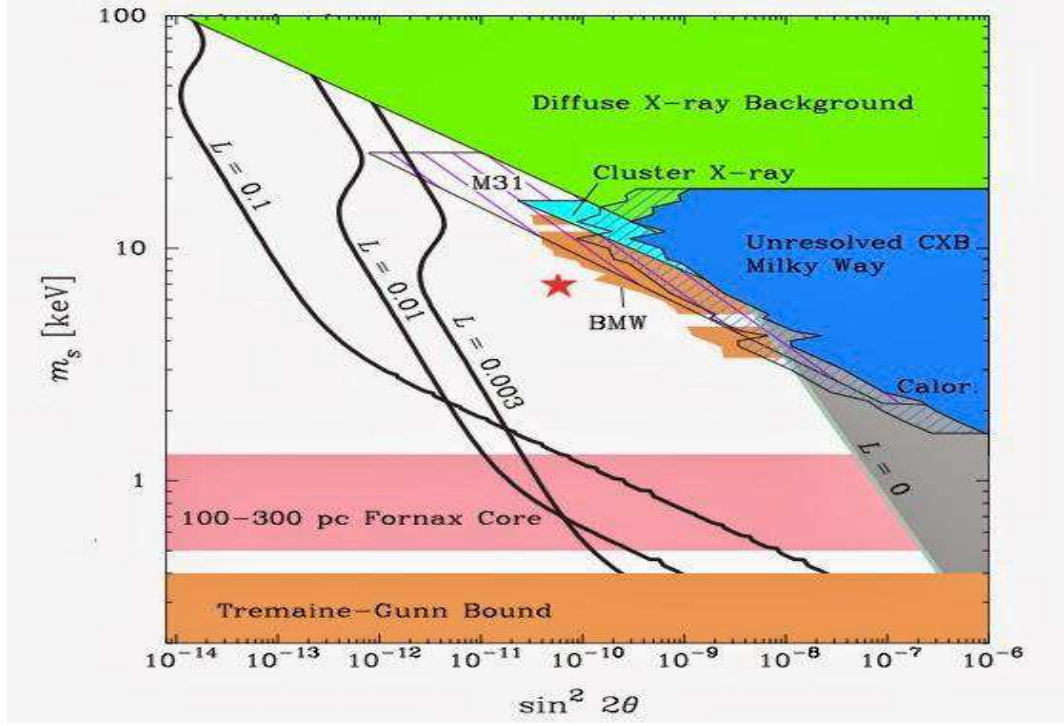


FIG. 7: Constraints on the sterile neutrino models from the literature. The full-sample line detection (assuming that the line is from sterile neutrino and that all dark matter is in sterile neutrino) is shown; error bar is statistical 90%. Historic constraints are taken from ref. [52]. Black curves show theoretical predictions for the Dodelson-Widrow mechanism assuming that sterile neutrinos constitute the dark matter with lepton numbers  $L=0, 0.003, 0.01, 0.1$ . See [52] for explanation of the various observational constraints. The Bulbul et al. [51] detection of the sterile neutrino indicated by a red star. The measurement lays at the boundary of the constraints from M31.



- Active neutrino:  $\sim$  mili eV
- Light sterile neutrino:  $\sim$  eV
- Dark Matter sterile neutrino:  $\sim$  keV
- Unstable sterile neutrino:  $\sim$  MeV....

This scheme may represent the future extension of the Standard Model of particle physics.

In order to falsify WDM, comprehensive theoretical calculations showing substructures, galaxy formation and evolution including the quantum WDM effects in the dynamical evolution are needed to contrast with the astronomical observations.

In such WDM theoretical calculations the quantum pressure must be necessarily included. These calculations should be performed matching the semiclassical Hartree-Fock (Thomas-Fermi) dynamics where the dimensionless phase-space density is high enough, namely,  $\hbar^3 Q/m^4 \gtrsim 0.1$  with the classical evolution dynamics where  $\hbar^3 Q/m^4 \ll 1$ . These are certainly not easy numerical calculations but they are unavoidable!

Richard P. Feynman foresaw the necessity to include quantum physics in simulations in 1981 [50]

**“I’m not happy with all the analyses that go with just the classical theory, because nature isn’t classical, dammit, and if you want to make a simulation of nature, you’d better make it quantum mechanical, and by golly it’s a wonderful problem, because it doesn’t look so easy.”**

Sterile neutrino detection depends upon the particle physics model. There are sterile neutrino models where the keV sterile is stable and thus hard to detect (see for example [30]).

Detection may proceed through astronomical observations of X-ray keV sterile neutrino decay from galaxy halos and by direct detection of sterile neutrinos in laboratory experiments.

Mare [34], Katrin [35, 36], ECHO [37], Project 8 [38], HOLMES and Ptolemy [41] are expected to provide bounds on the mixing angles. However, for a direct particle detection, a dedicated beta decay experiment and/or electron capture experiment seem necessary to find sterile neutrinos with mass in the keV range. In this respect, calorimetric techniques seem well suited.

The best nuclei for study are  $^{187}\text{Re}$  and Tritium for beta decay and  $^{163}\text{Ho}$  for electron capture. However, only Tritium has enough available energy  $Q$  to produce 7 keV sterile neutrinos.

The search of DM particles with mass around 7 keV is a promisory avenue for future trascendental discoveries.

- 
- [1] D. Boyanovsky, H J de Vega, N. G. Sanchez, Phys. Rev. **D 78**, 063546 (2008).
  - [2] H. J. de Vega, N. G. Sánchez, Phys. Rev. D85, 043516 (2012) and D85, 043517 (2012).
  - [3] C. Destri, H. J. de Vega, N. G. Sanchez, New Astronomy **22**, 39 (2013) and Astroparticle Physics, 46, 14 (2013).
  - [4] H. J. de Vega, P. Salucci, N. G. Sanchez, MNRAS, 442, 2717 (2014).
  - [5] H. J. de Vega, N. G. Sanchez, arXiv:1310.6355.
  - [6] G. Gilmore et al., Ap J, 663, 948 (2007).
  - [7] M. Walker, J. Peñarrubia, Ap. J. 742, 20 (2011).
  - [8] P. Salucci et al., MNRAS, 378, 41 (2007).
  - [9] H. J. de Vega, P. Salucci, N. G. Sanchez, New Astronomy **17**, 653 (2012) and references therein.
  - [10] J. D. Simon, M. Geha, Ap J, 670, 313 (2007) and references therein.
  - [11] J. P. Brodie et al., AJ, 142, 199 (2011). B. Willman and J. Strader, AJ, 144, 76 (2012). J. D. Simon et al., Ap. J. 733, 46 (2011) and references therein. J. Wolf et al., MNRAS, 406, 1220 (2010) and references therein. G. D. Martinez et al., Ap J, 738, 55 (2011).
  - [12] A. W. McConnachie, AJ, 144, 4 (2012).
  - [13] H. J. de Vega, N. G. Sánchez, Mon. Not. R. Astron. Soc. **404**, 885 (2010) and Int. J. Mod. Phys. **A 26**, 1057 (2011).
  - [14] W. B. Lin et al., PRL 86, 954 (2001). X-J Bi et al., PRD 80, 103502 (2009). Q Yuan et al., PRD 86, 103531 (2012).
  - [15] P. Colín, O. Valenzuela, V. Avila-Reese, Ap J, 542, 622 (2000). J. Sommer-Larsen, A. Dolgov, Ap J, 551, 608 (2001). L. Gao and T. Theuns, Science, 317, 1527 (2007). A. Schneider et al., MNRAS, 424, 684 (2012).
  - [16] M. R. Lovell et al., MNRAS, 420, 2318 (2012).
  - [17] A. V. Tikhonov et al., MNRAS, 399, 1611 (2009).
  - [18] E. Papastergis et al., Ap J, 739, 38 (2011), J. Zavala et al., Ap J, 700, 1779 (2009).

- [19] A. V. Macciò, S. Paduroiu, D. Anderhalden, A. Schneider, B. Moore, MNRAS, 424, 1105 (2012). S. Shao et al. arXiv:1209.5563, MNRAS. 430, 2346 (2013).
- [20] Highlights and conclusions of the Chalonge Colloquiums and Workshops: arXiv:1203.3562, arXiv:1109.3187, arXiv:1009.3494, arXiv:1007.2411 and the online presentations:  
<http://chalonge.obspm.fr/ProgrammeCIAS2014.html>  
<http://chalonge.obspm.fr/ProgrammeParis2014.html>
- [21] N. Menci, F. Fiore, A. Lamastra, ApJ, 766, 110 (2013).
- [22] R. Kennedy et al., MNRAS, 442, 2487 (2014).
- [23] C. Destri, H. J. de Vega, N. G. Sanchez, Phys. Rev. D88, 083512 (2013).
- [24] F. Munyaneza, P. L. Biermann, A & A, 458, L9 (2006). P. H. Chavanis, Phys. Rev. **E65**, 056123 (2002), P. H. Chavanis, Int. J. Mod. Phys. B20, 3113 (2006).
- [25] F. Marinacci et al., MNRAS 437, 1750 (2014). M. Schaller et al., arXiv:1409.8617 and arXiv:1409.8297.
- [26] Dama/Libra: R. Bernabei et al., arXiv:1301.6243, *Eur.Phys.J.* **C67** (2010) 39. CDMS-II: R. Agnese et al., arXiv:1304.4279, Z. Ahmed et al., *Science* **327** (2010) 1619, PRL **106** (2011) 131302. AMS: M. Aguilar et al., PRL, 110, 141102 (2013). CoGeNT: C. Aalseth et al., Phys.Rev.Lett. **107** (2011) 141301. CRESST: G. Angloher et al., *Eur.Phys.J.* **C72** (2012) 1971. XENON10: J. Angle et al., PRL **107** (2011) 051301, XENON100: E. Aprile et al., PRL **109** (2012) 181301.
- [27] P. L. Biermann et al. PRL (2009), P. Blasi, P. D. Serpico PRL (2009).
- [28] L D Landau and E M Lifshits, Statistical Mechanics, Elsevier, Oxford, 1980.
- [29] H J de Vega, O. Moreno, E. Moya, M. Ramón Medrano, N. Sánchez, Nucl. Phys. **B866**, 177 (2013).
- [30] A. Merle, arXiv:1302.2625, Int. J. Mod. Phys. D22, 1330020 (2013).
- [31] R N Mohapatra, P B Pal, 'Massive neutrinos in physics and astrophysics', World Scientific, Singapore, 2004.
- [32] M. Loewenstein, A. Kusenko, P. L. Biermann, Astrophys.J. 700 (2009) 426-435 M. Loewenstein, A. Kusenko, Astrophys.J. 714 (2010) 652 and 751 (2012) 82.
- [33] C. R. Watson et al. JCAP, 03, 018 (2012).
- [34] <http://mare.dfm.uninsubria.it/frontend/exec.php>
- [35] <http://www.katrin.kit.edu/>
- [36] S. Mertens et al. , Sensitivity of Next-Generation Tritium Beta-Decay Experiments for keV-Scale Sterile Neutrino, arXiv:1409.0920s; Wavelet Approach to Search for Sterile Neutrinos in Tritium  $\beta$ -Decay Spectra, arXiv:1410.7684.
- [37] Lecture by Loredana Gastaldo at the Chalonge Meudon Workshop 2014, <http://chalonge.obspm.fr/>
- [38] <http://www.npl.washington.edu/project8/>
- [39] <http://xenia.msfc.nasa.gov/>
- [40] <http://astro-h.isas.jaxa.jp/> , T. Takahashi et al. arXiv:1210.4378.
- [41] Betts, S. et al., Arxiv 1307.4738.  
 Lecture by Chris Tully at the Chalonge Meudon Workshop 2014, <http://chalonge.obspm.fr/>
- [42] A. Kogut et al., JCAP 07, 025 (2011).
- [43] G. Raffelt, S. Zhou, PRD 83, 093014 (2011).
- [44] G. Steigman, Adv. in High Energy Phys. 268321 (2012) and Phys. Rev. D 87 (2013) 103517.
- [45] E. W. Kolb, M. S. Turner, 'The Early Universe', Addison-Wesley, 1990, Redwood City.
- [46] P. A. R. Ade et al., Planck 2013 results. XVI. arXiv:1303.5076.
- [47] J. Kopp et al. JHEP 1305:050, 2013 and references therein.
- [48] S. N. Gninenko, Phys. Rev. D85, 051702(R) (2012) and references therein.
- [49] M. Drewes, Int J Mod. Phys. E22, 1330019 (2013).
- [50] R. P. Feynman, Lecture at the 1st. Conference on Physics and Computation, MIT 1981, Int. J. Theor. Phys. **21**,467(1982).
- [51] E. Bulbul et al. ApJ 789, 23 (2014).
- [52] K Abazajian, astro2010, The Astronomy and Astrophysics Decadal Survey, 2010, 1.
- [53] K Abazajian, Phys. Rev. Lett. 112, 161303 (2014).